




# Redshift Dependence of the Low-energy Spectral Index of Gamma-Ray Bursts Revisited

Xiao-Li Zhang<sup>1</sup> , Yong-Feng Huang<sup>2,3,4</sup> , and Ze-Cheng Zou<sup>2</sup> 

<sup>1</sup>Department of Physics, Nanjing University, Nanjing 210023, China

<sup>2</sup>School of Astronomy and Space Science, Nanjing University, Nanjing 210023, China; [hyf@nju.edu.cn](mailto:hyf@nju.edu.cn)

<sup>3</sup>Key Laboratory of Modern Astronomy and Astrophysics (Nanjing University), Ministry of Education, Nanjing 210023, China

<sup>4</sup>Xinjiang Astronomical Observatory, Chinese Academy of Sciences, Urumqi 830011, China

Received 2023 June 12; revised 2023 July 23; accepted 2023 August 4; published 2023 October 25

## Abstract

A negative correlation was found to exist between the low-energy spectral index and the redshift of gamma-ray bursts (GRBs) by Amati et al. It was later confirmed by Geng & Huang and Gruber et al., but the correlation was also found to be quite dispersive when the sample size was significantly expanded. In this study, we have established two even larger samples of GRBs to further examine the correlation. One of our samples consists of 316 GRBs detected by the Swift satellite, and the other one consists of 80 GRBs detected by the Fermi satellite. It is found that there is no correlation between the two parameters for the Swift sample, but there does exist a weak negative correlation for the Fermi sample. The correlation becomes even more significant when the spectral index at the peak flux is considered. It is argued that the absence of the correlation in the Swift sample may be due to the fact that Swift has a very narrow energy response so that it could not measure the low-energy spectral index accurately enough. Further studies based on even larger GRB samples are solicited.

*Key words:* (stars:) gamma-ray burst: general – methods: statistical – catalogs

## 1. Introduction

Gamma-ray bursts (GRBs) are the most violent stellar explosions. They were initially discovered in 1967 (Klebesadel et al. 1973) by the Vela Satellites. Up to now, they have been intensively studied for more than forty years since more and more GRBs are discovered (Qin et al. 2021; Yuan et al. 2022a; Liu et al. 2022). Generally, GRBs are believed to be triggered by the death of massive stars or by the merger of binary compact stars. The empirical correlation between different parameters of GRBs is one of the present interesting objects. For instance, the correlation between  $E_p$  (the peak energy) and  $E_{\text{iso}}$  (the equivalent isotropic energy), i.e., the so-called Amati relation is investigated by Amati et al. (2002, 2009), Virgili et al. (2012), Azzam & Alothman (2013), Geng & Huang (2013) and Demianski et al. (2017). The correlation between  $E_p$  (the peak energy) and  $L_p$  (the peak luminosity), i.e., the so-called Yonetoku relation is investigated by Yonetoku et al. (2004), Ghirlanda et al. (2005) and Zhang et al. (2012). Yonetoku et al. (2010) and Tsutsui et al. (2013) have discussed both relations. Furthermore, Wang et al. (2020) has even discussed other more empirical correlations beyond the above relations.

The redshift ( $z$ ) is an important parameter of GRBs. Many people have studied the relation between  $z$  and other parameters. For example, Zhang et al. (2014a) investigated the correlations between  $z$  and  $L_{\text{iso}}$ ,  $E_{\text{iso}}$ ,  $E_{p,\text{rest}}$ ,  $E_{p,\text{obs}}$

( $E_{p,\text{obs}} = E_{p,\text{rest}}/(1+z)$ ) (also see Sakamoto et al. 2011; Ukwatta et al. 2012). Especially, they found a positive correlation between  $z$  and  $L_{\text{iso}}$  for the Swift GRBs. Wei & Gao (2003) and Zitouni et al. (2014) studied the  $z$ - $E_{\text{iso}}$  relation and the  $z$ - $L_{\text{iso}}$  relation. Moreover, the relation between  $z$  and  $L_p$  has also been investigated by many researchers (Lloyd-Ronning et al. 2002; Goldstein 2012; Salvaterra et al. 2012; Zhang et al. 2014b; Zitouni et al. 2018).

The low-energy spectral index,  $\alpha$ , is also an important parameter that characterizes the prompt emission of GRBs. Geng et al. (2018) have tried to derive the value of  $\alpha$  through numerical simulations by considering the synchrotron emission mechanism. Especially, the correlation between  $\alpha$  and  $E_p$  has been studied by many researchers (Gruber et al. 2014; Li et al. 2019; Duan & Wang 2020; Li 2022). Tang et al. (2019) also investigated the correlation between  $\alpha$  and  $E_{\text{iso}}$ .

Interestingly, Amati et al. (2002) found that there seems to be a negative correlation between  $z$  and  $\alpha$ , which reads  $\log \alpha = (-0.78 \pm 0.13)\log(1+z) + (0.39 \pm 0.04)$ . Here the symbol  $\log$  means the logarithm base is 10. Their study is conducted on a sample that only includes nine GRBs. Later, Geng & Huang (2013) and Gruber et al. (2014) confirmed the existence of such a correlation, which was updated as  $\log \alpha = (-0.42 \pm 0.07)\log(1+z) + (0.11 \pm 0.02)$ . Their sample consists 65 GRBs, which is much larger than that of Amati et al. (2002). However, Geng & Huang (2013) also

noted that the correlation is quite dispersive. It is thus necessary to further examine the existence of such a  $z - \alpha$  correlation. In this study, we will further expand the GRB sample to include 316 GRBs detected by Swift and 80 GRBs detected by Fermi. We then use this significantly expanded sample to check the correlation between  $z$  and  $\alpha$ .

The structure of this article is organized as follows. A detailed description of the selection of the data sample is provided in Section 2. The correlation between the low-energy spectral index and the redshift, and some other relations between various parameter pairs, are explored in Section 3. Finally, our conclusions and discussion are presented in Section 4.

## 2. Sample

GRBs detected by Swift and Fermi are used in this study. Two conditions are applied in selecting the appropriate GRBs. First, the redshift of the burst should be available. Second, the spectrum should be well defined. The time-averaged spectra of GRBs are usually fitted with three kinds of functions: a single power-law function, a cutoff power-law function, and the so-called Band Function (Band et al. 1993). Most of the GRBs spectra can be well fitted by the Band function, which is expressed as

$$F(E) = A \begin{cases} \left(\frac{E}{100 \text{ keV}}\right)^{-\alpha} \exp\left[-\frac{(2-\alpha)E}{E_p}\right], & E < \frac{-(\alpha-\beta)E_p}{2-\alpha}; \\ \left(\frac{E}{100 \text{ keV}}\right)^{-\beta} \exp(\alpha-\beta) \left[\frac{-(\alpha-\beta)E_p}{100 \text{ keV}(2-\alpha)}\right]^{-(\alpha-\beta)}, & E \geq \frac{-(\alpha-\beta)E_p}{2-\alpha}, \end{cases} \quad (1)$$

where  $E$  is the photon energy. There are four parameters in this equation: the scaling factor ( $A$ ), the low- and high-energy spectral indices ( $\alpha$  and  $\beta$ , respectively), and the peak photon energy ( $E_p$ ). In our notation,  $\alpha$  and  $\beta$  are positive by using their absolute values. We have collected all the spectrum parameters of those Swift and Fermi GRBs with the redshift measured.

Fermi has a very wide energy band, i.e., 8–35,000 keV. So, Fermi GRBs are usually best fitted by the Band function, which is represented by the lower-energy spectral index ( $\alpha$ ) and the high-energy spectral index ( $\beta$ ). On the other hand, the Swift/BAT detector has a very narrow energy response of 15–150 keV so that Swift GRBs are generally best fitted by a single power-law function or by a cutoff power-law function. In these cases, the derived power-law index could be regarded as a useful representation of the low-energy spectral index ( $\alpha$ ), since it is measured in the soft  $\gamma$ -ray range. Note that for the Swift GRBs, the  $\beta$  parameter is completely unavailable.

For the Swift GRBs, the relevant data are acquired by inquiring on the NASA Swift website.<sup>5</sup> As a result, a total

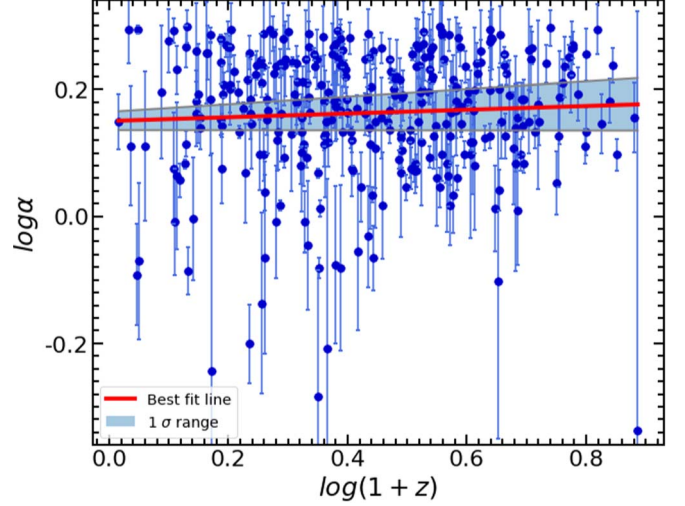


**Figure 1.** Swift sample on the  $\log \alpha - \log(1+z)$  plane. Here  $\alpha$  is the low-energy spectral index and  $z$  is the redshift. The solid line is the best fit result and the shaded region shows the corresponding  $1\sigma$  range.

number of 316 GRBs are included in our Swift sample, all of which have the necessary redshift and spectrum data. The time span of these GRBs ranges from 2005 January 26, to 2023 January 16.

For the Fermi GRBs, the data are collected mainly by consulting NASA's HEASARC (the High Energy Astrophysics Science Archive Research Center) database.<sup>6</sup> As a useful supplement, 24 bursts were taken from Jochen Greiner's online GRB catalog.<sup>7</sup> Finally, our Fermi sample consists of 80 GRBs. The time span of these Fermi GRBs ranges from 2008 September 5 to 2018 July 20.

## 3. Correlations

In this section, the Swift and Fermi GRB samples are employed to explore the empirical correlations concerning  $\alpha$  and  $z$ . Figure 1 shows the Swift sample on the  $\log \alpha - \log(1+z)$  plane. Generally, we see that the data points are quite scattered and there is no obvious correlation between the two parameters. The solid line in Figure 1 is the best-fit result of the data points, which corresponds to  $\log \alpha = (0.029 \pm 0.030) \log(1+z) + (0.15 \pm 0.014)$ . But note that it has a very small correlation coefficient of  $r = 0.055$ , which indicates that essentially no correlation exists. Here, the error ranges of the best-fit parameters are given in  $1\sigma$  ranges throughout this paper.

In Figure 2, we plot the Fermi GRB sample on the  $\log \alpha - \log(1+z)$  plane in the left panel. The observational data points are also fitted with a linear function. Note that GRB 120712A seems to be an obvious outlier on the plane, whose

<sup>5</sup> <https://swift.gsfc.nasa.gov/archive/>

<sup>6</sup> <https://heasarc.gsfc.nasa.gov/db-perl/W3Browse/>

<sup>7</sup> <https://www.mpe.mpg.de/~jcg/grbgen.html>

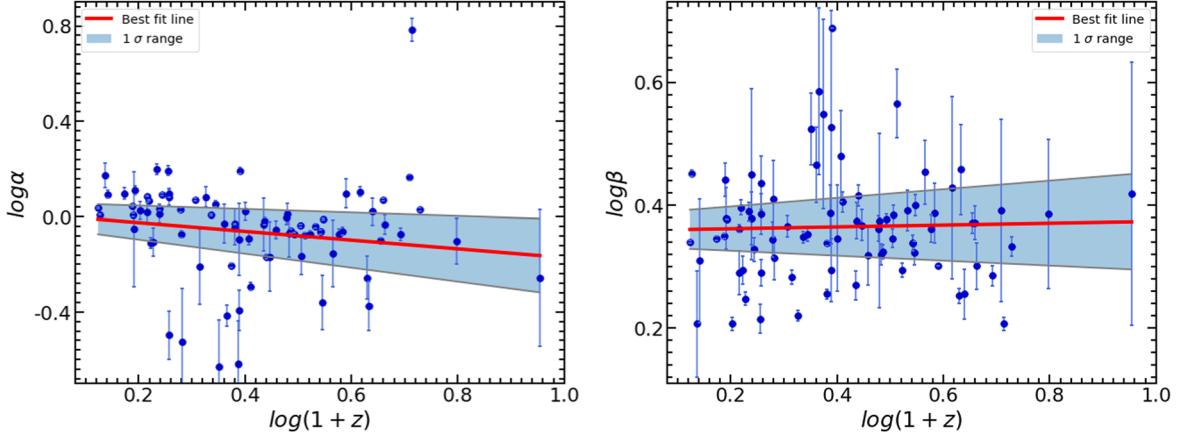


**Figure 2.** The spectral index plotted against redshift for the Fermi GRB sample. The left panel shows the low-energy spectral index ( $\alpha$ ) vs. redshift ( $z$ ). The right panel shows the high-energy spectral index ( $\beta$ ) vs. redshift ( $z$ ). The solid lines correspond to the best fit results to the data points and the shaded regions show the corresponding  $1\sigma$  ranges. Note that in the left panel, the isolated data point (GRB 120712A) on the top is not included in the linear fit since it is an obvious outlier.

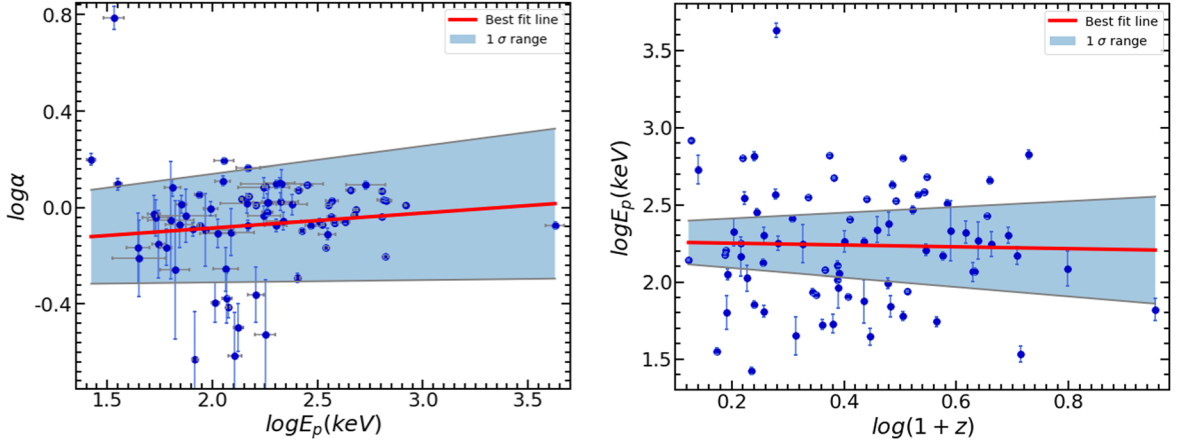


**Figure 3.**  $\alpha$  vs.  $E_p$  (left panel) and  $E_p$  vs.  $z$  (right panel) for the Fermi GRBs. The solid lines correspond to the best fit results to the data points and the shaded regions show the corresponding  $1\sigma$  ranges. Note that in the left panel, the isolated data point (GRB 120712A) on the top is not included in the linear fit since it is an obvious outlier.

low-energy spectral index is  $\alpha = 6.1 \pm 0.67$ . We exclude this event in the fitting procedure. Interestingly, we could see that there is a negative correlation between  $\alpha$  and  $z$ . The best-fit result is  $\log \alpha = (-0.18 \pm 0.11)\log(1+z) + (0.012 \pm 0.049)$ , with a correlation coefficient of  $r = -0.19$ . But note that this expression, especially the slope of the line (i.e.,  $-0.18$ ), is quite different from those of previous studies. Also, the correlation here is generally very weak. As a comparison, the right panel of Figure 2 shows the Fermi GRB sample on the  $\log \beta - \log(1+z)$  plane. We see that there is no correlation between the two parameters, which is consistent with previous results of Geng & Huang (2013). The best-fit line corresponds to  $\log \beta = (0.015 \pm 0.055)\log(1+z) + (0.36 \pm 0.025)$ , with a very small correlation coefficient of  $r = 0.031$ . Comparing the two panels of Figure 2, it is quite clear that the low-energy spectral index ( $\alpha$ ) is

still obviously different from the high energy index ( $\beta$ ) when they are plotted against the redshift.

The Fermi GRBs have well-measured  $E_p$  data. So, in Figure 3, we plot them on the  $\alpha - E_p$  plane and the  $E_p - z$  plane. We see that there is no obvious correlation either between  $\alpha$  and  $E_p$ , or between  $E_p$  and  $z$ . The results are also somewhat different from those of previous studies. For example, Geng & Huang (2013) argued that  $E_p$  and  $z$  are positively correlated. Note that GRB 120712A is again an obvious outlier in this figure and is not included in the fitting procedure.

Since the peak time of the flux is an important stage of a GRB, we have also investigated the features of the peak flux parameters. For this purpose, we could only adopt the Fermi GRB sample, since peak flux parameters are not available for

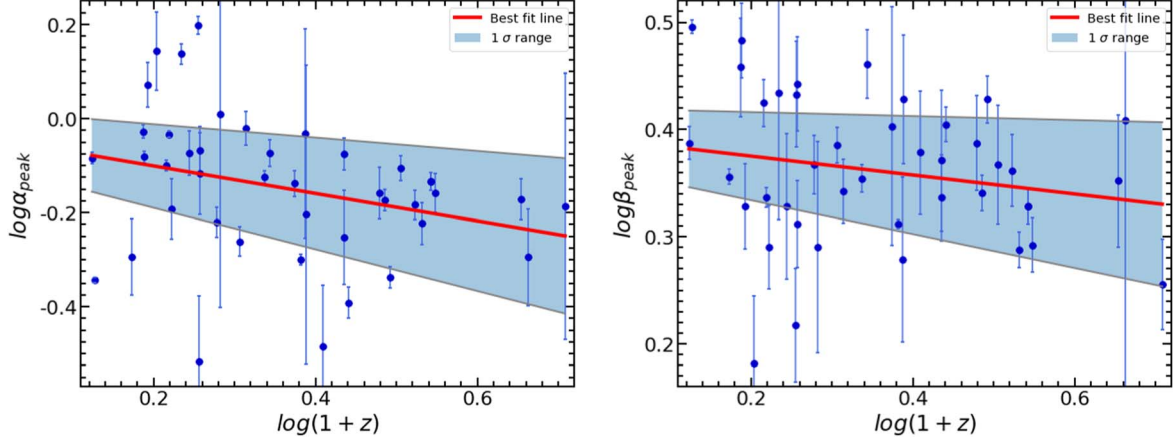


**Figure 4.** The peak flux spectral indices plotted against the redshift for the Fermi GRB sample. The left panel shows the low-energy spectral index at the peak flux moment ( $\alpha_{\text{peak}}$ ) vs. the redshift. The right panel shows the corresponding high-energy spectral index ( $\beta_{\text{peak}}$ ) vs. the redshift. The solid lines correspond to the best fit results to the data points and the shaded regions show the corresponding  $1\sigma$  ranges.

many Swift GRBs. Here, the low-energy spectral index at the peak flux of the burst is denoted as  $\alpha_{\text{peak}}$ . Correspondingly, the high-energy spectral index and peak photon energy at the peak flux are denoted as  $\beta_{\text{peak}}$  and  $E_{\text{peak}}$ , respectively.

In the left panel of Figure 4, the Fermi GRB sample are plotted on the  $\log \alpha_{\text{peak}} - \log(1+z)$  plane. Here, we could see that there is an obvious negative correlation between  $\alpha_{\text{peak}}$  and  $z$ , although it is still quite scattered. The best-fit result is  $\log \alpha_{\text{peak}} = (-0.29 \pm 0.15)\log(1+z) + (-0.042 \pm 0.059)$ , with a correlation coefficient of  $r = -0.29$ . Comparing with the slope of  $-0.42$  previously derived for the  $\log \alpha - \log(1+z)$  correlation (Geng & Huang 2013), here the slope of the  $\log \alpha_{\text{peak}} - \log(1+z)$  relation (i.e.,  $-0.29$ ) is significantly flatter. The right panel of Figure 4 shows the Fermi GRB sample on the  $\log \beta_{\text{peak}} - \log(1+z)$  plane. There is also a weak correlation between the two parameters, which can be best fitted as  $\log \beta_{\text{peak}} = (-0.088 \pm 0.070)\log(1+z) + (0.39 \pm 0.027)$ , with a correlation coefficient of  $r = -0.20$ . Note that the data points in the right panel are much dispersive as compared with those in the left panel.

Figures 2 and 4 show that there is a weak correlation between the low-energy spectral index and the redshift. Especially, the  $\alpha - z$  relation is much less significant than the  $\alpha_{\text{peak}} - z$  relation. A natural speculation is that  $\alpha$  and  $\alpha_{\text{peak}}$  should be positively connected, then the above two relations should be largely similar. The reason that leads to such a difference thus deserves to be examined. Figure 5 plots  $\alpha$  against  $\alpha_{\text{peak}}$  for the Fermi sample. The solid line shows the case when  $\alpha$  equals  $\alpha_{\text{peak}}$ . We see that  $\alpha$  and  $\alpha_{\text{peak}}$  are not strictly connected, which could explain their different dependence on the redshift. It reflects the fact that the  $\gamma$ -ray spectrum is highly variable during a GRB.

Figure 6 illustrates the relations between  $\alpha_{\text{peak}}$ ,  $E_{\text{peak}}$ , and  $z$ . There is a weak correlation between  $E_{\text{peak}}$  and  $z$ , which reads

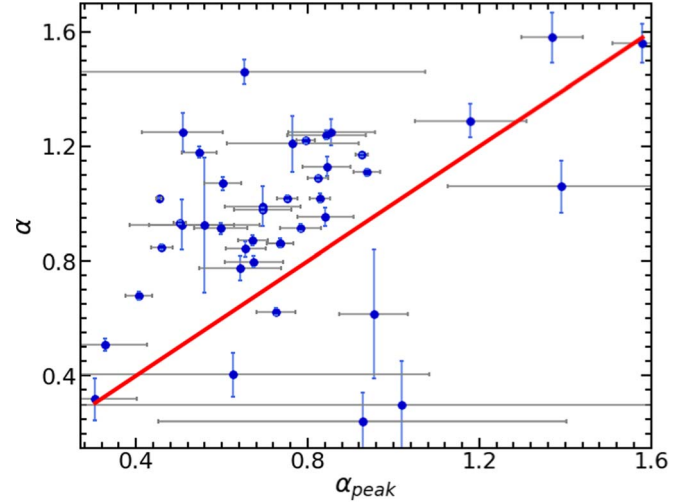


**Figure 5.**  $\alpha_{\text{peak}}$  plotted vs.  $\alpha$  for the Fermi GRB sample. The solid line corresponds to the case of  $\alpha = \alpha_{\text{peak}}$ .

$\log E_{\text{peak}} = (0.26 \pm 0.33)\log(1+z) + (2.30 \pm 0.13)$ , with the correlation coefficient being  $r = 0.13$ . Similarly, there is also a weak correlation between  $\alpha_{\text{peak}}$  and  $E_{\text{peak}}$ , which corresponds to  $\log \alpha_{\text{peak}} = (-0.072 \pm 0.071)\log E_{\text{peak}} + (0.0088 \pm 0.17)$ , with the correlation coefficient being  $r = -0.16$ .

Swift/BAT has a relatively narrow passband, i.e., 15–150 keV. Therefore, the measured spectral index should correspond to the low-energy spectral index of the Band function. Some GRBs are simultaneously detected by Swift and Fermi satellites. It is then interesting to know whether the spectral index measured by Swift is consistent with that measured by Fermi. In Figure 7, we have screened out all the overlapping GRBs between the Swift sample and Fermi sample, and compared their spectral indices. Here,  $\alpha^S$  is the



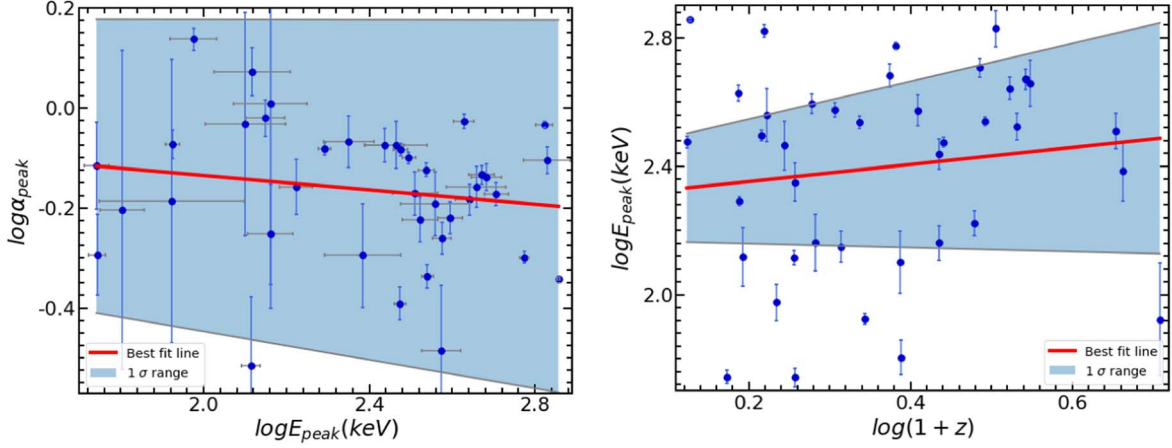


**Figure 6.**  $\alpha_{\text{peak}}$  plotted vs.  $E_{\text{peak}}$  (left panel), and  $E_{\text{peak}}$  plotted vs.  $z$  (right panel) for the Fermi GRB sample. The solid lines correspond to the best fit results and the shaded regions show the corresponding  $1\sigma$  ranges.

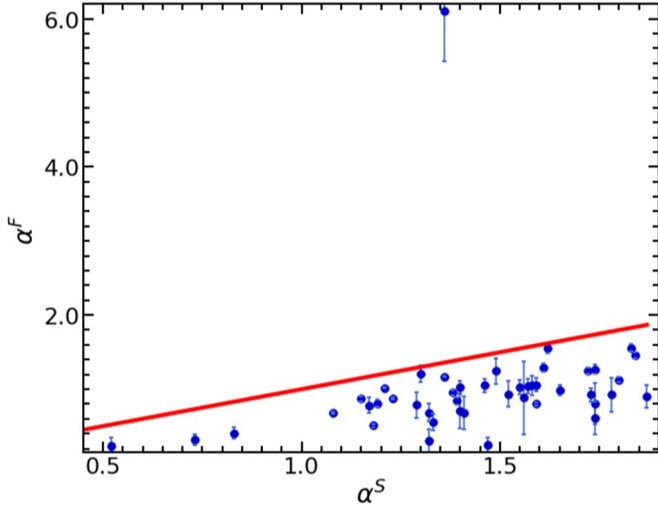


**Figure 7.** The low-energy spectral index measured by Fermi ( $\alpha^F$ ), plotted vs. the spectral index measured by Swift ( $\alpha^S$ ). Note that only overlapping GRBs between the Fermi sample and the Swift sample are shown here. The solid line corresponds to the case of  $\alpha^F = \alpha^S$ .

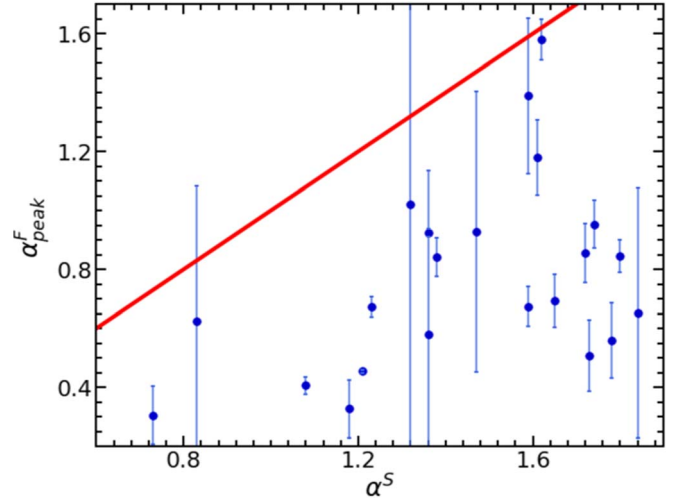


**Figure 8.** The low-energy spectral index at the peak flux measured by Fermi ( $\alpha_{\text{peak}}^F$ ), plotted vs. the spectral index measured by Swift ( $\alpha^S$ ). Note that only overlapping GRBs between the Fermi sample and the Swift sample are shown here. The solid line corresponds to the case of  $\alpha_{\text{peak}}^F = \alpha^S$ .

spectral index measured by Swift, while  $\alpha^F$  is the low-energy spectral index measured by Fermi. We see that  $\alpha^S$  and  $\alpha^F$  are not equal for each event. The former is systematically larger than the latter. Also, the data points are quite scattered. For these overlapping GRBs, we have also compared their  $\alpha^S$  with their low-energy spectral index at the peak flux as measured by Fermi ( $\alpha_{\text{peak}}^F$ ). The results are shown in Figure 8. Similarly, we see that  $\alpha^S$  again is generally larger than  $\alpha_{\text{peak}}^F$ . Figures 7 and 8 clearly show that different detectors could generate very different results for the spectrum of even the same GRB, which indicates that acquiring the spectra of GRBs is still a very difficult task. The different  $\alpha - z$  correlations of different

GRB samples could thus be caused by the systematic distortion in measuring the spectral indices.

#### 4. Discussion and Conclusions

In this study, we use the Swift GRBs and Fermi GRBs to explore the possible correlation between the low-energy spectral index and the redshift. For the Swift GRB sample, it is found that there is no correlation between  $\alpha$  and  $z$  (see Figure 1). On the other hand, there is a weak correlation between  $\alpha$  and  $z$  for the Fermi GRB sample (see Figure 2). The correlation is even more obvious when the peak flux spectrum

is considered, i.e., when  $\alpha_{\text{peak}}$  is plotted versus  $z$  (Figure 4). The different features of the two samples may be caused by the different energy responses of the two detectors. The energy band of Fermi is very wide (8–35,000 keV), which ensures that it can present a much better description of the spectra of the detected GRBs. However, the Swift/BAT has a very narrow energy response (15–150 keV). As a result, the spectra of Swift GRBs are usually best fitted by a single power-law function or by a cutoff power-law function. In these cases, the power-law spectral index may significantly deviate from the true low-energy spectral index. This conjecture was confirmed when the spectra of the overlapping GRBs of the two samples were scrutinized. It is found that when a GRB is simultaneously detected by both Fermi and Swift, then the spectral index reported by Swift is usually quite different from the low-energy spectral index ( $\alpha$ ) reported by Fermi (Figures 7 and 8). It reflects the difficulty in spectral observations of GRBs.

Amati et al. (2002) argued that the correlation between  $\alpha$  and  $z$  is  $\log \alpha = (-0.78 \pm 0.13)\log(1+z) + (0.39 \pm 0.04)$ . Note that their sample size is very small. Later, Geng & Huang (2013) updated the correlation as  $\log \alpha = (-0.42 \pm 0.07)\log(1+z) + (0.11 \pm 0.02)$  using a significantly expanded sample. We see that the slope between  $\log \alpha$  and  $\log(1+z)$  becomes much flatter, and the correlation is also very dispersive. According to our current study, the correlation is now  $\log \alpha = (-0.18 \pm 0.11)\log(1+z) + (0.012 \pm 0.049)$  for the Fermi sample, and it is  $\log \alpha_{\text{peak}} = (-0.29 \pm 0.15)\log(1+z) + (-0.042 \pm 0.059)$  for the peak flux spectrum. The correlation becomes even flatter and more dispersive. Anyway, based on this study, we can conclude that a weak correlation does exist between  $\alpha$  and  $z$ . Also, further study on this issue still deserves to be conducted in the future. For this purpose, detectors with a relatively wide energy response are necessary to accurately measure the exact spectra of GRBs. We note that the Einstein Probe, a wide field (3600 square degrees) X-ray satellite that is scheduled to be launched in late 2023 (Yuan et al. 2018, 2022b), might be very helpful in this aspect. Einstein Probe is very sensitive in X-rays and may markedly help increase the sample size of well-localized GRBs.

### Acknowledgments

This study was supported by the National Natural Science Foundation of China (grant Nos. 12233002, 12041306, 12147103, and U1938201), by the National SKA Program of

China (No. 2020SKA0120300), by the National Key R&D Program of China (2021YFA0718500), and by the Youth Innovations and Talents Project of Shandong Provincial Colleges and Universities (grant No. 201909118).

### ORCID iDs

Xiao-Li Zhang  <https://orcid.org/0000-0002-3877-9289>  
Yong-Feng Huang  <https://orcid.org/0000-0001-7199-2906>  
Ze-Cheng Zou  <https://orcid.org/0000-0002-6189-8307>

### References

- Amati, L., Frontera, F., & Guidorzi, C. 2009, *A&A*, **508**, 173  
Amati, L., Frontera, F., Tavani, M., et al. 2002, *A&A*, **390**, 81  
Azzam, W. J., & Alothman, M. J. 2013, *IJAA*, **3**, 372  
Band, D., Matteson, J., Ford, L., et al. 1993, *ApJ*, **413**, 281  
Demianski, M., Piedipalumbo, E., Sawant, D., & Amati, L. 2017, *A&A*, **598**, A112  
Duan, M.-Y., & Wang, X.-G. 2020, *ApJ*, **890**, 90  
Geng, J. J., & Huang, Y. F. 2013, *ApJ*, **764**, 75  
Geng, J.-J., Huang, Y.-F., Wu, X.-F., Zhang, B., & Zong, H.-S. 2018, *ApJS*, **234**, 3  
Ghirlanda, G., Ghisellini, G., Firmani, C., Celotti, A., & Bosnjak, Z. 2005, *MNRAS*, **360**, L45  
Goldstein, A. 2012, PhD thesis, University of Alabama, Huntsville  
Gruber, D., Goldstein, A., Weller von Ahlefeld, V., et al. 2014, *ApJS*, **211**, 12  
Klebesadel, R. W., Strong, I. B., & Olson, R. A. 1973, *ApJL*, **182**, L85  
Li, L. 2022, *ApJ*, **941**, 27  
Li, L., Geng, J.-J., Meng, Y.-Z., et al. 2019, *ApJ*, **884**, 109  
Liu, H.-Y., Wang, X.-G., Xin, L.-P., et al. 2022, *RAA*, **22**, 065002  
Lloyd-Ronning, N. M., Fryer, C. L., & Ramirez-Ruiz, E. 2002, *ApJ*, **574**, 554  
Qin, S.-M., Jiang, L.-Y., & Wang, X.-G. 2021, *RAA*, **21**, 072  
Sakamoto, T., Barthelmy, S. D., Baumgartner, W. H., et al. 2011, *ApJS*, **195**, 2  
Salvaterra, R., Campana, S., Vergani, S. D., et al. 2012, *ApJ*, **749**, 68  
Tang, C.-H., Huang, Y.-F., Geng, J.-J., & Zhang, Z.-B. 2019, *ApJS*, **245**, 1  
Tsutsui, R., Yonetoku, D., Nakamura, T., Takahashi, K., & Morihara, Y. 2013, *MNRAS*, **431**, 1398  
Ukwatta, T. N., Dhuga, K. S., Stamatikos, M., et al. 2012, *MNRAS*, **419**, 614  
Virgili, F. J., Qin, Y., Zhang, B., & Liang, E. 2012, *MNRAS*, **424**, 2821  
Wang, F., Zou, Y.-C., Liu, F., et al. 2020, *ApJ*, **893**, 77  
Wei, D. M., & Gao, W. H. 2003, *MNRAS*, **345**, 743  
Yonetoku, D., Murakami, T., Nakamura, T., et al. 2004, *ApJ*, **609**, 935  
Yonetoku, D., Murakami, T., Tsutsui, R., et al. 2010, *PASJ*, **62**, 1495  
Yuan, H.-Y., Lü, H.-J., Li, Y., et al. 2022a, *RAA*, **22**, 075011  
Yuan, W., Zhang, C., Chen, Y., & Ling, Z. 2022b, Handbook of X-ray and Gamma-ray Astrophysics, Vol. 86 (Singapore: Springer), 1  
Yuan, W., Zhang, C., Ling, Z., et al. 2018, *Pro. SPIE*, **10699**, 1069925  
Zhang, F.-W., Shao, L., Fan, Y.-Z., & Wei, D.-M. 2014a, *Ap&SS*, **350**, 691  
Zhang, Z. B., Chen, D. Y., & Huang, Y. F. 2012, *ApJ*, **755**, 55  
Zhang, Z. B., Liu, H. C., Jiang, L. Y., & Chen, D. Y. 2014b, *JApA*, **35**, 561  
Zitouni, H., Guessoum, N., AlQassimi, K. M., & Alaryani, O. 2018, *Ap&SS*, **363**, 223  
Zitouni, H., Guessoum, N., & Azzam, W. J. 2014, *Ap&SS*, **351**, 267